Topological spin texture in Janus monolayers of the chromium trihalides Cr(I, X)_{3}

Changsong Xu, Junsheng Feng, Sergei Prokhorenko, Yousra Nahas, Hongjun Xiang, and L. Bellaiche

Phys. Rev. B **101**, 060404 — Published 10 February 2020

DOI: 10.1103/PhysRevB.101.060404

Topological Spin Textures in Janus Monolayers of Chromium Trihalides $Cr(I,X)_3$

Changsong Xu,[1,*] Junsheng Feng,[2,*] Sergei Prokhorenko,[1] Yousra Nahas,[1] Hongjun Xiang,[3,4,†] and L. Bellaiche[1,‡]

[1] *Physics Department and Institute for Nanoscience and Engineering, University of Arkansas, Fayetteville, Arkansas 72701, USA*

[2] *School of Physics and Materials Engineering, Hefei Normal University, Hefei 230601, P. R. China*

[3] *Key Laboratory of Computational Physical Sciences (Ministry of Education), State Key Laboratory of Surface Physics, and Department of Physics, Fudan University, Shanghai, 200433, China*

[4] *Collaborative Innovation Center of Advanced Microstructures, Nanjing 210093, P. R. China*

Topological magnetic states are promising for ultra-dense memory and logic devices. Recent progresses in two-dimensional magnets encourage the idea to realize topological states, such as skrmions and merons, in freestanding monolayers. However, monolayers such as CrI_3 lack Dzyaloshinskii-Moriya interactions (DMI) and thus do not naturally exhibit skyrmions/merons but rather a ferromagnetic state. Here we propose the fabrication of $Cr(I,X)_3$ Janus monolayers, in which the Cr atoms are covalently bonded to the underlying I ions and top-layer Br or Cl atoms. By performing first-principles calculations and Monte-Carlo simulations, we identify strong enough DMI, which leads to not only helical cycloid phases, but also to topologically nontrivial states, such as the intrinsic domain wall skyrmions in $Cr(I,Br)_3$ and the magnetic-field-induced bimerons in $Cr(I,Cl)_3$. Microscopic origins of such spin textures are revealed as well.

Novel spin textures, such as skyrmions and merons, are nano-scale spin clusters with topological stability, and are promising for advanced spintronics [1–3]. One requirement toward such applications is that the hosting materials should be thin films, so that the nano size of the spin clusters can be taken full advantage of. Besides previous studies on skyrmionic states of bulk MnSi [4–7], recent works focused on ultrathin films, such as skyrmion states in FeGe [8, 9] and rare-earth ion garnet [10, 11] and meron states in $Co_8Zn_9Mn_3$ [12], which all take advantage of the Dzyaloshinskii-Moriya interaction (DMI) arising from relativistic spin-orbit coupling (SOC). However, no skyrmionic state has ever been reported to intrinsically exist in free-standing *monolayers*, to the best of our knowledge. Two-dimensional (2D) semiconducting magnets, such as monolayer CrI_3 [13], are recently attracting much attention due to their novel physics and rich applications [14]. The ferromagnetic monolayer CrI_3 crystalizes in honeycomb lattice made of edge-sharing octahedra. Its ferromagnetic order is stabilized by an out-of-plane anisotropy [13], which arises from single ion anisotropy (SIA) and Kitaev-type exchange coupling that both result from the SOC of its heavy ligands [15, 16]. However, the ingredient DMI is absent between the most strongly coupled first nearest neighbor (1st NN) Cr-Cr pairs, because the inversion center between the two Cr atoms prevents its existence [17].

Here we propose a novel approach that consists in fabricating Janus monolayers of chromium trihalides $Cr(I,X)_3$ (X = Br, Cl). One example of Janus monolayers is the transition metal dichalcogenides MoSSe, which originates from the well-known monolayer MoS_2 but with one layer of S being substituted by Se. Such Janus monolayer is experimentally achievable, since MoSSe has been reproducibly obtained using different methods [18, 19], which strongly suggests the feasibility of also creating $Cr(I,X)_3$ Janus monolayers. In this manuscript, we apply density functional theory (DFT) and parallel tempering Monte Carlo (PTMC) simulations to study the magnetic interactions and to reveal novel spin textures of two Janus monolayers, namely $Cr(I,Br)_3$ and $Cr(I,Cl)_3$, as well as the prototype CrI_3 (see structural schematics in Figs. 1a and 1b). As we will show, these Janus monolayers exhibit not only strong enough DMI, but also a decrease in magnetic anisotropy energy (MAE), which both contribute to stabilizing helical, skyrmion and even bimeron states. We also demonstrate that the presence of Kitaev interaction and the application of magnetic field both benefit to the emergence of novel spin textures in these $Cr(I,X)_3$ Janus monolayers.

Hamiltonian and magnetic parameters. We consider the following Hamiltonian for describing the magnetic interactions of the $Cr(I,Br)_3$ and $Cr(I,Cl)_3$ Janus monolayers, as well as the prototype CrI_3 monolayer, using the generalized matrix form up to the second nearest neighbors (2nd NN) for the spins, $\mathbf{S}$:

$$\mathcal{H} = \frac{1}{2}\sum_{n=1,2}\sum_{(i,j)_n} \mathbf{S}_i \cdot \mathcal{J}_{n,ij} \cdot \mathbf{S}_j + \sum_i \mathbf{S}_i \cdot \mathcal{A}_{ii} \cdot \mathbf{S}_i \ , \qquad (1)$$

where the first term is the exchange coupling that runs over all first $(i,j)_1$ and second $(i,j)_2$ NN Cr pairs, respectively, and the second term represents SIA that runs over all Cr sites. $\mathcal{J}$ and $\mathcal{A}$ are 3×3 matrices, for which the elements can be extracted using the four-state energy mapping method and density-functional theory (DFT) (see supplementary materials (SM) [20] for details). The $\mathcal{J}$ matrices can be further decomposed into an isotropic parameter J', the symmetric Kitaev term K [15] and the antisymmetric DMI vector $\mathbf{D}$ [21]; and the $\mathcal{A}$ matrix simply reduces to its A_{zz} components by symmetry. The

* Contributed equally to this work
† hxiang@fudan.edu.cn
‡ laurent@uark.edu

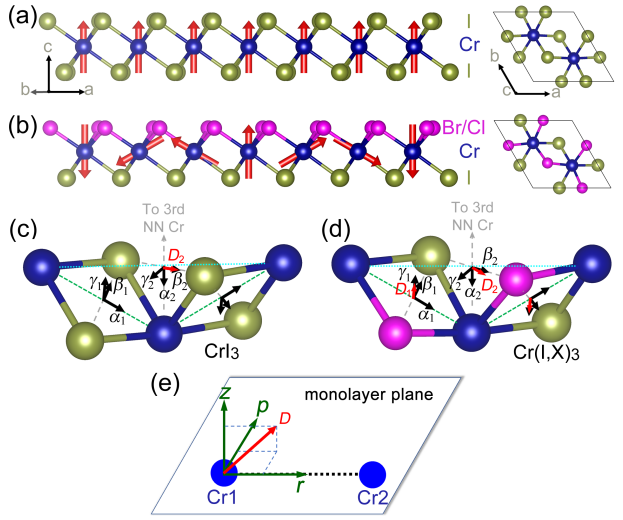

FIG. 1. Panel (a) and (b) display the side and top views of CrI_3 and $Cr(I,X)_3$, respectively. The red arrows in (a) and (b) schematize the FM and helix spin configurations, respectively; (c) and (d) illustrate the eigenvectors $\{\alpha\beta\gamma\}$ of Kitaev interactions and the directions of DMI vectors of CrI_3 and $Cr(I,X)_3$, respectively; (e) schematizes the DM vector being decomposed into its $\{rpz\}$ components.

Hamiltonian can then be rewritten as

$$\mathcal{H} = \frac{1}{2}\sum_{n=1,2}\sum_{(i,j)_n}\{J'_n\mathbf{S}_i\cdot\mathbf{S}_j + K_n S_i^\gamma S_j^\gamma + \mathbf{D}_{n,ij}\cdot(\mathbf{S}_i\times\mathbf{S}_j)\} + \sum_i A_{zz}(S_i^z)^2 \ , \quad (2)$$

where $J' = (J'_\alpha + J'_\beta)/2$, $K = J'_\gamma - J'$ and S^γ is the γ component of $\mathbf{S}$ in a local basis $\{\alpha, \beta, \gamma\}$ that results from the diagonalization of the symmetric part of $\mathcal{J}$ (see Fig. 1c, 1d and SM [20] for details about Kitaev interaction). The directions of the DMI vectors $\mathbf{D}$ are illustrated in Figs. 1c and 1d. Specifically, the $\mathbf{D}_1$ vectors of both $Cr(I,X)_3$ are perpendicular to the Cr_2IX plane, which satisfy Moriya's rule [17] and thus testify the accuracy of our calculations. The $\mathbf{D}_2$ vectors are basically pointing from one bridging I to the other I or X. Note that we further define another isotropic parameter as $J = (J_{xx} + J_{yy} + J_{zz})/3$, which is equivalent to the J coefficient involved in the commonly used $J\mathbf{S}_i\cdot\mathbf{S}_j$ term. Such isotropic J is thus different from J' and its ratio with the DMI parameter ($|D/J|$) can provide information about the existence of magnetic skyrmions or not.

Let us now look at the precise values of the magnetic parameters obtained from DFT and four-state method [15, 21, 23, 24]. As shown in Table I, both J_1 and J_2 yield negative values, which imply ferromagnetism (FM) for all investigated systems, which is consistent with the measured ferromagnetism of CrX_3, with X = Cl, Br and I [13, 25, 26]. The J_1, K_1 and A_{zz} parameters all decrease in magnitude when the X ion of $Cr(I,X)_3$ varies from I to Cl, via Br. This decrease in J_1 results from the shrinking of lattice constants [27], while that of K_1 and A_{zz} root in the weakening of the SOC strength (as consistent with the location of I, Br and Cl in the periodic table). On the other hand, the J_2 and K_2 coefficients show no significant changes with the X ion. Moreover, the Janus monolayers $Cr(I,Br)_3$ and $Cr(I,Cl)_3$ exhibit remarkable D_1 values of 0.270 meV and 0.194 meV, respectively, while the prototype CrI_3 has no finite D_1, as aforementioned. Such values, altogether with J_1, yield large $|D_1/J_1|$ ratios of 0.150 for $Cr(I,Br)_3$ and 0.194 for $Cr(I,Cl)_3$, which are within the typical range of 0.1-0.2 known to generate skyrmionic phases [2]. Note that a very recent theoretical study proposed the application of electric field to monolayer CrI_3, in order to break the inversion center and induce DMI [28]. Although this method is clever, the electric field has a weak effect in generating DMI, as an extremely large electric field of 2 V/nm leads to a small $|D_1/J_1|$ of 0.071, which hinders the actual creation of skyrmions. Notably, our three investigated systems also show non-negligible D_2 values, which leads to $|D_2/J_2|$ ratios comparable to their 1st NN counterparts, as detailed in Table I. The significant $|D_1/J_1|$ and $|D_2/J_2|$ ratios of $Cr(I,Br)_3$ and $Cr(I,Cl)_3$ demonstrate that the fabrication of Janus monolayers is an effective way to induce considerable DMI and is thus promising to create magnetic skyrmions.

TABLE I. Magnetic parameters of CrI_3, $Cr(I,Br)_3$ and $Cr(I,Cl)_3$ monolayers [22]. Note that $S = 3/2$ is used when extracting the magnetic parameters. The energy unit is in meV.

Mag. Para.	CrI_3	$Cr(I,Br)_3$	$Cr(I,Cl)_3$
J_1	-2.218	-1.800	-0.983
K_1	0.847	0.505	0.422
D_1	0	0.270	0.191
$\|D_1/J_1\|$	0	0.150	0.194
J_2	-0.638	-0.673	-0.754
K_2	0.078	0.075	0.094
D_2	0.135	0.114	0.138
$\|D_2/J_2\|$	0.212	0.169	0.183
A_{zz}	-0.262	-0.124	-0.029

Another important factor that affects the formation of topological states is the magnetic anisotropy energy (MAE), which is defined as the energy difference between out-of-plane FM (zFM) and in-plane FM (xFM) states, $\epsilon = E_{\mathrm{zFM}} - E_{\mathrm{xFM}}$, where $\epsilon < 0$ (> 0, respectively) favors out-of-plane (in-plane, respectively) FM. Figure S1a display the MAE calculated using the model energy of Eq. (2) with the parameters of Table 1. The prototype CrI_3, with ϵ = -0.693 meV/Cr, favors strong out-of-plane anisotropy and $Cr(I,Br)_3$, with ϵ = -0.218 meV/Cr, exhibits mild out-of-plane anisotropy. In contrast, $Cr(I,Cl)_3$ shows weak in-plane anisotropy since ϵ = 0.111 meV/Cr [29]. As we will see latter, such differences in anisotropy between $Cr(I,Br)_3$ and $Cr(I,Cl)_3$ plays a role on the morphology of the spin textures.

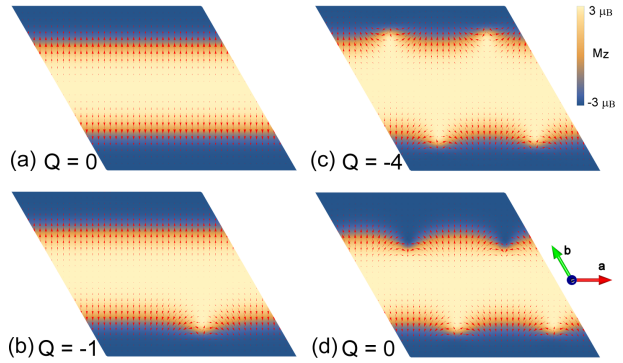

FIG. 2. Magnetic structures and topological charges of $Cr(I,Br)_3$. (a) shows the out-of-plane Néel-type cycloid; (b) illustrates one DWS at one domain boundary; (c) and (d) each hosts four DWS and are also energetically degenerate but with different Q. The color map applies to the *out-of-plane* component of the spin vectors ("spin-in" and "spin-out", for negative (dark) and positive (bright) z-components, respectively) while the arrows characterize the *in-plane* components of the spin vectors.

Intrinsic domain wall skyrmion in $Cr(I,Br)_3$. As detailed in the Method section, parallel tempering Monte Carlo (PTMC) simulations using the Hamiltonian of Eq. (1) are performed over a 50×50×1 supercell to find spin structures with low energies. These latter spin structures are then further relaxed with the conjugate gradient (CG) method, until arriving at energy minima. Such optimization scheme guarantees the converged spin structures to be either metastable states or the ground state at the temperature of zero Kelvin.

Practically, the ground state of $Cr(I,Br)_3$ is determined to be out-of-plane ferromagnetism (zFM), of which the energy is set to be zero. The first metastable state (the convention of terminology here is that the nth metastable state has the $(n+1)$th lowest energy) of $Cr(I,Br)_3$ is an out-of-plane Néel-type cycloid structure, as shown in Fig. 2a, with an energy of 0.056 meV/Cr. Its propagation direction is symmetrically equivalent along $\mathbf{(a+2b)}$, $\mathbf{(2a+b)}$ and $\mathbf{(b-a)}$. Moreover, the in-plane components of the spin vectors and the propagation direction form angles of ∼5.9° around the middle of domains (bright and dark zones) and ∼3.2° near the domain walls. Such cycloid structure yields no finite topological charge Q that is defined as $Q = \frac{1}{4\pi}\int \mathbf{m}\cdot(\frac{\partial \mathbf{m}}{\partial x})\times(\frac{\partial \mathbf{m}}{\partial y})dxdy$, where $\mathbf{m}$ is the unit vector lying along the local magnetic moment's direction.

On the other hand, novel topological states with finite Q are found as the second and even higher metastable states. As shown in Fig. 2b, near the lower bright-dark domain boundary, the spin vectors not only behave as the aforementioned Néel-type cycloid, but also rotate clockwise in the film plane and form a point defect. The in-plane components of such defect is reminiscent of a domain wall skyrmion (DWS) [30], or precisely, a slice of the latter. The in-plane rotation, together with the out-of-plane cycloidal behavior, renders Q = -1 and is thus topologically equivalent to the common axially symmetric skyrmion [4–7]. We thus refer to this special defect as a DWS for simplicity. Such DWS state of Fig. 2b has an energy of 343.5 meV/DWS with respect to the ground state and 63.8 meV/DWS with respect to the cycloid phase.

Moreover, it is found that either the upper or the lower domain boundary can host multiple DWS, as shown in Fig. 2c. The 50×50×1 supercell can thus host up to four DWS. Interestingly, when the in-plane components of the spin vectors rotate anticlockwise, it forms a domain wall antiskyrmion, with $Q = +1$. As shown in Fig. 2d, the upper domain boundary hosts two antiskyrmions and the lower one hosts two skyrmions, which results in the total topological charge being $Q = 0$. Interestingly, either a skyrmion or an antiskyrmion is found to cost an energy of 63.8 meV/DWS with respect to the cycloid state. In fact, the energy is linearly increasing with simply the number of skyrmions, as shown in Fig. S2c. It is also found here that skyrmions and anti-skyrmions can not exist at the same domain wall, since they tend to annihilate with each other which would in fact lead to the transformation to the cycloidal state (resulting in $Q = 0$) [31].

In order to reveal the microscopic origin of the aforementioned spin textures, DMI vectors are decomposed into their $\{rpz\}$ components. As shown in Fig. 1e, the $\hat{\mathbf{r}}$-axis is along the Cr-Cr bond direction and thus in-plane; the $\hat{\mathbf{p}}$ -axis is perpendicular to $\hat{\mathbf{r}}$ and also in-plane, and the $\hat{\mathbf{z}}$-axis is the out-of-plane direction. As shown in Table SII, for $Cr(I,Br)_3$, this decomposition gives $\mathbf{D}_1$ = (0, -0.226, -0.147) meV for the Cr-Cr pair that is along $\mathbf{(a-b)/2}$ and $\mathbf{D}_2$ = (0.080, -0.040, -0.071) meV. As detailed in Sec. SII and Table SIII of SM, by switching these components on and off in the simulations, it is found that (i) D_1^p and D_2^p both favor the Néel-type cycloid of Fig. 2a, which is consistent with previous knowledge [32]; (ii) D_1^z favors in-plane canting, which results in the 3.2° to 5.9° in-plane angles of the cycloid; (iii) D_2^r leads to a slight energy gain when creating DWS on a cycloid, due to the changes in out-of-plane components of spins; while (iv) K_1 and A_{zz} are the driving forces to create DWS on a cycloid, since they favor the extra out-of-plane components with respect to the perfect cycloid, which explains the energetic degeneracy between clockwise and anticlockwise DWS.

Magnetic field induced bimeron states in $Cr(I,Cl)_3$. As consistent with its positive MAE, the ground state of $Cr(I,Cl)_3$ is determined to be in-plane zigzag-canted FM, as shown in Fig. 3a. The spin vectors at the A and B sites of the honeycomb lattice make an angle of 6.7°, which is in good agreement with the 6.2° that is directly obtained from DFT on a unit cell. Comparing to the xFM state, such canting renders an in-plane perpendicular moment of 0.15 μ_B/Cr, with an energy lowering of 0.024 meV/Cr. Such zigzag-canted FM state is degenerate when the main component of the magnetization is along the $\mathbf{a}$ direction (which is precisely our x-direction),

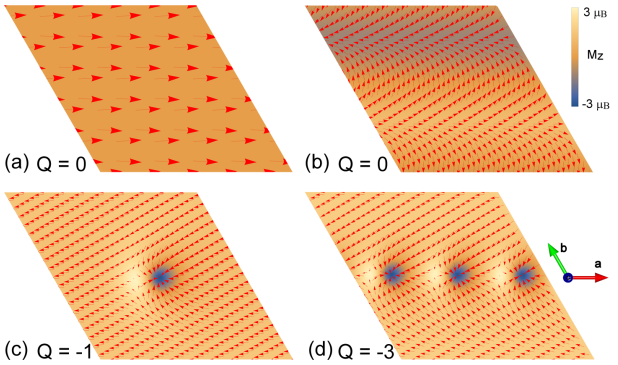

FIG. 3. Magnetic structures and topological charges of $Cr(I,Cl)_3$. (a) shows the in-plane zigzag canted FM state; (b) illustrates the in-plane cycloidal structure; (c) and (d) display one and three bimerons, respectively, with an out-of-plane magnetic field B of 0.8 T. See Fig. 2 for explanations of the color map and the vectors.

or along **b** and **(a + b)** directions.

The first metastable state is a mostly in-plane cycloidal structure superimposed with small out-of-plane components forming a waved spin pattern, as shown in Fig. 3b [33]. Note also that the zigzag canting of the ground state exists in such cycloid phase too. Such cycloidal structure has an energy higher by 0.026 meV/Cr from the ground state and is degenerate for propagation directions being along **(a + 2b)**, **(2a + b)** or **(b − a)** directions.

Skyrmionic states are not found to be "naturally" stable in $Cr(I,Cl)_3$ within our Hamiltonian, partially due to the relatively strong in-plane anisotropy. An out-of-plane magnetic field B is then applied to compensate the in-plane anisotropy that arises from the original DFT-derived magnetic parameters (K and A_{zz}). It is numerically found that, for $B > 0.65$ T, zFM is energetically more favorable than in-plane FM. However, the magnetic field (< 2 T) does not polarize the spins to the fully out-of-plane direction, but rather renders the in-plane zigzag-canted FM now possessing an out-of-plane component. The previously metastable cycloid state can not survive and transform to such FM state when $B > 0.2$ T.

Interestingly, topologically nontrivial bimeron states can be stabilized in $Cr(I,Cl)_3$ with a compensative magnetic field between 0.5 and 1.3 T. A meron/antimeron can be viewed as half of a skyrmion/antiskyrmion (and thus has a half integer topological charge Q) embedded in a background made of in-plane dipoles [12, 34]. Note also that a bimeron [35–38], which is a pair of merons or antimerons, is sometimes referred to as asymmetric skyrmion [39], double-pair skyrmion [40], or in-plane skyrmion [3, 41] too. Although micrometer-sized merons have been widely reported in permalloys [42–45], merons with nanometric sizes have only been very recently observed in $Co_8Zn_9Mn_3$ [12]. The merons/bimerons not only induce emergent electromagnetism and thus novel Hall effects [1], but are also promising for the next generation of memory devices [43]. Practically, for a magnetic field of 0.8 T and as shown in Fig. 3c, we identify two merons, one being a core-down vortex and the other one being a core-up antivortex. Such two merons form a close pair with a diameter of ∼10.5 nm and each has Q = -$\frac{1}{2}$. Such meron pair is thus precisely a bimeron with Q = -1. Due to the energy lowering from magnetic field, this bimeron state has an energy of -63.7 meV/bimeron with respect to the zigzag FM phase of Fig. 3a, while it is still metastable with an energy of 74.4 meV/bimeron with respect to ground state under 0.8 T magnetic field. Moreover, it is found that up to three bimerons can be stabilized within the 50×50×1 supercell and the energy also linearly increases with the topological charges in $Cr(I,Cl)_3$, as shown in Fig. S2c.

Again, we decompose DMI vectors into their {rpz} components to investigate their specific effects on spin textures. As shown in Table SII, $Cr(I,Cl)_3$ possesses $\mathbf{D}_1$ = (0, -0.154, -0.113) meV and $\mathbf{D}_2$ = (0.095, -0.054, -0.085) meV. As detailed in Sec. SII and Table SIII of SM, it is determined that (i) D_1^z leads to the zigzag canting in both the ground state of Fig. 3a and the cycloid phase of Fig. 3b; (ii) D_1^p and D_2^p not only result in the out-of-plane waved spin pattern of the cycloid phase of Fig. 3b, but also work together with the anisotropy and result in the bimerons of Fig. 3c-d (note that such anisotropy arises from interplay among SIA, Kitaev interaction and the magnetic field); while (iii) other DMI components have either negligible or even no contributions.

In summary, we propose the fabrication of $Cr(I,X)_3$ (X = Br, Cl) Janus monolayers to induce large DMI and subsequent topological spin states. By combining DFT and MC simulations, we find that $Cr(I,Br)_3$ can intrinsically host metastable domain wall skyrmion phases, while a bimeron state of $Cr(I,Cl)_3$ can be stabilized by applying an out-of-plane magnetic field. The Kitaev interaction, for the first time, is found critical to stabilize DWS and bimerons, as it contributes to the MAE and adds to the disorder of the systems (see SM for details). Our study thus suggests a feasible approach to create topological spin textures in semiconducting magnets consisting of chromium trihalides Janus monolayers. Such presently predicted topological phases are not only useful for memory and logic devices, but can also be promising for energy storage[46].

ACKNOWLEDGMENTS

C.X. and L.B. thank Office of Basic Energy Sciences under contract ER-46612 and an Impact Grant from Arkansas Research Alliance. S.P., Y.N. and L.B. thank the financial support of the DARPA Grant No. HR0011727183-D18AP00010 (TEE Program). Y.N. and L.B. also acknowledge support of the ARO grant W911NF-16-1-0227. H.X. is supported by NSFC (11825403), the Special Funds for Major State Basic Research (2015CB921700), Program for Professor of Special Appointment (Eastern Scholar), Qing Nian Ba Jian Pro-

gram, and Fok Ying Tung Education Foundation. J.F. acknowledges the support from Anhui Provincial Natural Science Foundation (1908085MA10). The Arkansas High Performance Computing Center (AHPCC) is also acknowledged.

[1] N. Nagaosa and Y. Tokura, Nature nanotechnology **8**, 899 (2013).

[2] A. Fert, V. Cros, and J. Sampaio, Nature nanotechnology **8**, 152 (2013).

[3] K. Everschor-Sitte, J. Masell, R. M. Reeve, and M. Kläui, Journal of Applied Physics **124**, 240901 (2018).

[4] S. Heinze, K. Von Bergmann, M. Menzel, J. Brede, A. Kubetzka, R. Wiesendanger, G. Bihlmayer, and S. Blügel, Nature Physics **7**, 713 (2011).

[5] S. Mühlbauer, B. Binz, F. Jonietz, C. Pfleiderer, A. Rosch, A. Neubauer, R. Georgii, and P. Böni, Science **323**, 915 (2009).

[6] A. Neubauer, C. Pfleiderer, B. Binz, A. Rosch, R. Ritz, P. Niklowitz, and P. Böni, Phys. Rev. Lett. **102**, 186602 (2009).

[7] C. Pappas, E. Lelievre-Berna, P. Falus, P. Bentley, E. Moskvin, S. Grigoriev, P. Fouquet, and B. Farago, Phys. Rev. Lett. **102**, 197202 (2009).

[8] X. Yu, N. Kanazawa, Y. Onose, K. Kimoto, W. Zhang, S. Ishiwata, Y. Matsui, and Y. Tokura, Nature materials **10**, 106 (2011).

[9] S. Huang and C. Chien, Phys. Rev. Lett. **108**, 267201 (2012).

[10] C. O. Avci, E. Rosenberg, L. Caretta, F. Büttner, M. Mann, C. Marcus, D. Bono, C. A. Ross, and G. S. Beach, Nature nanotechnology , 1 (2019).

[11] Q. Shao, Y. Liu, G. Yu, S. K. Kim, X. Che, C. Tang, Q. L. He, Y. Tserkovnyak, J. Shi, and K. L. Wang, Nature Electronics **2**, 182 (2019).

[12] X. Yu, W. Koshibae, Y. Tokunaga, K. Shibata, Y. Taguchi, N. Nagaosa, and Y. Tokura, Nature **564**, 95 (2018).

[13] B. Huang, G. Clark, E. Navarro-Moratalla, D. R. Klein, R. Cheng, K. L. Seyler, D. Zhong, E. Schmidgall, M. A. McGuire, D. H. Cobden, W. Yao, D. Xiao, P. Jarillo-Herrero, and X. Xu, Nature **546**, 270 (2017).

[14] M. Gibertini, M. Koperski, A. Morpurgo, and K. Novoselov, Nature nanotechnology **14**, 408 (2019).

[15] C. Xu, J. Feng, H. Xiang, and L. Bellaiche, npj Computational Materials **4**, 57 (2018).

[16] J. L. Lado and J. Fernández-Rossier, 2D Materials **4**, 035002 (2017).

[17] T. Moriya, Phys. Rev. **120**, 91 (1960).

[18] A.-Y. Lu, H. Zhu, J. Xiao, C.-P. Chuu, Y. Han, M.-H. Chiu, C.-C. Cheng, C.-W. Yang, K.-H. Wei, Y. Yang, et al., Nature nanotechnology **12**, 744 (2017).

[19] J. Zhang, S. Jia, I. Kholmanov, L. Dong, D. Er, W. Chen, H. Guo, Z. Jin, V. B. Shenoy, L. Shi, et al., ACS nano **11**, 8192 (2017).

[20] See supplemetary materials at, which cite [15, 21, 23, 24, 26, 47–58].

[21] C. Xu, B. Xu, B. Dupé, and L. Bellaiche, Phys. Rev. B **99**, 104420 (2019).

[22] The second nearest neighbors DMI of CrI_3 are also listed in Table I, and have the potential to result in noncollinear spin textures. ().

[23] H. Xiang, E. Kan, S.-H. Wei, M.-H. Whangbo, and X. Gong, Phys. Rev. B **84**, 224429 (2011).

[24] H. Xiang, C. Lee, H.-J. Koo, X. Gong, and M.-H. Whangbo, Dalton Transactions **42**, 823 (2013).

[25] B. Morosin and A. Narath, The Journal of Chemical Physics **40**, 1958 (1964).

[26] M. Kim, P. Kumaravadivel, J. Birkbeck, W. Kuang, S. G. Xu, D. Hopkinson, J. Knolle, P. McClarty, A. Berdyugin, M. B. Shalom, et al., arXiv preprint arXiv:1902.06988 (2019).

[27] The net negative and thus ferromagnetic (FM) J_1 results from the competition between Cr-Cr direct antiferromagnetic (AFM) coupling and Cr-X-Cr indirect FM coupling. The Cr-Cr distance becomes shorter via the shrinking of the lattice constants. Consequently, the direct AFM coupling is enhanced, while the changes to indirect FM coupling is relatively small, so that the total ferromagnetism is weaken and J_1 thus becomes smaller in magnitude [15, 59]. ().

[28] A. K. Behera, S. Chowdhury, and S. R. Das, arXiv preprint arXiv:1903.08797 (2019).

[29] Note that Fig. 2a also displays the ϵ directly calculated from DFT, that agree rather well with those obtained by the model – which thus further testifies the accuracy of our model Hamiltonian ().

[30] R. Cheng, M. Li, A. Sapkota, A. Rai, A. Pokhrel, T. Mewes, C. Mewes, D. Xiao, M. De Graef, and V. Sokalski, Physical Review B **99**, 184412 (2019).

[31] Moreover, it is found that the DWS can not be induced by magnetic field at zero temperature, since mild magnetic field increase the energy of DWS, while strong out-of-plane magnetic field polarize the spin patterns to zFM state. ().

[32] G. Yin, Y. Li, L. Kong, R. K. Lake, C.-L. Chien, and J. Zang, Physical Review B **93**, 174403 (2016).

[33] Note that such spin arrangement is reminiscent of the spin organization of $BiFeO_3$ that consists of an in-plane cycloidal structure and an out-of-plane waved spin pattern [60]. ().

[34] S.-Z. Lin, A. Saxena, and C. D. Batista, Physical Review B **91**, 224407 (2015).

[35] X. Zhang, M. Ezawa, and Y. Zhou, Scientific reports **5**, 9400 (2015).

[36] C. Heo, N. S. Kiselev, A. K. Nandy, S. Blügel, and T. Rasing, Scientific reports **6**, 27146 (2016).

[37] Y. Kharkov, O. Sushkov, and M. Mostovoy, Physical review letters **119**, 207201 (2017).

[38] B. Göbel, A. Mook, J. Henk, I. Mertig, and O. A. Tretiakov, Physical Review B **99**, 060407 (2019).

[39] A. Leonov and I. Kézsmárki, Physical Review B **96**, 014423 (2017).

[40] Y.-K. Liu and S.-J. Yang, New Journal of Physics **19**, 063037 (2017).

[41] K.-W. Moon, J. Yoon, C. Kim, and C. Hwang, arXiv preprint arXiv:1811.12552 (2018).

[42] T. Shinjo, T. Okuno, R. Hassdorf, K. Shigeto, and

T. Ono, Science **289**, 930 (2000).
[43] C. Phatak, A. K. Petford-Long, and O. Heinonen, Physical review letters **108**, 067205 (2012).
[44] S. Wintz, C. Bunce, A. Neudert, M. Körner, T. Strache, M. Buhl, A. Erbe, S. Gemming, J. Raabe, C. Quitmann, et al., Physical review letters **110**, 177201 (2013).
[45] A. Tan, J. Li, A. Scholl, E. Arenholz, A. Young, Q. Li, C. Hwang, and Z. Qiu, Physical Review B **94**, 014433 (2016).
[46] Y. Tserkovnyak and J. Xiao, Phys. Rev. Lett. **121**, 127701 (2018).
[47] G. Kresse and D. Joubert, Phys. Rev. B **59**, 1758 (1999).
[48] P. E. Blöchl, Phys. Rev. B **50**, 17953 (1994).
[49] W. Kohn and L. J. Sham, Phys. Rev. **140**, A1133 (1965).
[50] Y. Miyatake, M. Yamamoto, J. Kim, M. Toyonaga, and O. Nagai, Journal of Physics C: Solid State Physics **19**, 2539 (1986).
[51] M. R. Hestenes and E. Stiefel, Methods of conjugate gradients for solving linear systems, Vol. 49 (NBS Washington, DC, 1952).
[52] B. Berg and M. Lüscher, Nuclear Physics B **190**, 412 (1981).
[53] G. P. Müller, M. Hoffmann, C. Disselkamp, D. Schürhoff, S. Mavros, M. Sallermann, N. S. Kiselev, H. Jónsson, and S. Blügel, arXiv preprint arXiv:1901.11350 (2019).
[54] A. Kitaev, Annals of Physics **321**, 2 (2006).
[55] G. Jackeli and G. Khaliullin, Phys. Rev. Lett. **102**, 017205 (2009).
[56] J. Chaloupka, G. Jackeli, and G. Khaliullin, Phys. Rev. Lett. **105**, 027204 (2010).
[57] A. Leonov and M. Mostovoy, Nature communications **6**, 8275 (2015).
[58] A. N. Bogdanov and D. Yablonskii, Zh. Eksp. Teor. Fiz **95**, 178 (1989).
[59] X. Li and J. Yang, Journal of Materials Chemistry C **2**, 7071 (2014).
[60] D. Rahmedov, D. Wang, J. Íñiguez, and L. Bellaiche, Phys. Rev. Lett. **109**, 037207 (2012).